ATLAS-GUIDED PROBABILISTIC DIFFUSION-TENSOR FIBER TRACTOGRAPHY

Philip A Cook, Hui Zhang, Suyash P Awate and James C Gee

Penn Image Computing and Science Lab, Department of Radiology,
University of Pennsylvania, PA 19104, USA

ABSTRACT

We demonstrate the use of a diffusion tensor atlas to perform probabilistic tractography in diffusion tensor data. The tensors from eleven subjects are normalized into a common space by optimizing the similarity between tensors explicitly. The distribution of tensor orientations in the atlas space forms a prior distribution for the fiber orientation that is defined by the local anatomy, in contrast to previous curvature priors that restrict the local curvature of all tracts equally. We demonstrate the method in a single subject and compare tracking with a uniform prior, with a curvature prior, and with the atlas prior. The atlas information allows us to track further along the fornix and cingulum than the other priors.

Index Terms— Diffusion, tensor, probabilistic tractography, atlas

1. INTRODUCTION

Streamline tractography methods [1] aim to trace the path of white matter fiber tracts using the local fiber-orientation estimates derived from diffusion-weighted MRI. Uncertainty in fiber tracking comes from several sources, including noise, partial volumes within voxels, and complex fiber architecture that cannot be modeled by the diffusion tensor [2]. Heuristic priors on the local fiber orientation, such as a restriction on the curvature of the fiber pathway [3], or spatial regularization of diffusion tensors in local neighborhoods [4], are often used to reduce erroneous streamline traces. This work leverages an atlas of diffusion-tensor images to inform the prior probability of the local fiber orientation. The prior is evaluated as part of a Bayesian framework for probabilistic tractography.

2. MATERIALS AND METHODS

2.1. Data Acquisition

Twelve adult subjects were scanned in a Siemens Trio 3T scanner. Reconstructed voxel dimensions were 2.2 mm isotropic on a grid of 112×112, with 57 contiguous slices. The DWI protocol was 12 measurements at $b = 0$ and 30 at $b = 1000\,\mathrm{s\,mm^{-2}}$, each at independent gradient orientations spread isotropically on the sphere. The b=1000 measurements were repeated three times, giving a total of 102 DW images including those at $b = 0$. A multi-channel head coil was used with Siemens GRAPPA parallel imaging (factor 2.5).

We thank the National Institutes of Health for funding this work through grants NS045839, HD046159, HD042974 and MH068066. We thank Sumei Wang, Elias Melhem, and Murray Grossman, University of Pennsylvania, for acquiring the human brain data used in this work.

2.2. Atlas construction

The white matter atlas is generated from the DT images of eleven subjects using an iterative procedure [5] that leverages a high-dimensional tensor-based registration algorithm to explicitly optimize tensor orientation [6] The atlas contains eleven diffusion tensors in each voxel, each with a principal eigenvector $\vec{e}_1$. Once the tensors from all subject images are mapped into a common space, the dyadic tensor [7]

$$D_y = \frac{1}{11}\sum_{i=1}^{11} \vec{e}_{1i}\vec{e}_{1i}^{T}\,, \tag{1}$$

is calculated in each voxel. This tensor is distinct from the diffusion tensor in that it contains only orientation information about the mean and variance of the principal directions from the subjects. D_y has eigenvalues $t_1 \geq t_2 \geq t_3$, where $t_1 + t_2 + t_3 = 1$, when the tensors from all subjects are perfectly aligned, $t_1 = 1$ and when they are exactly uniformly distributed, $t1 = t2 = t3 = 1/3$.

2.3. Bayesian PDF estimation

The tractography algorithm is based on the Bayesian framework presented by Friman et al [8]. We use the "constrained model of the diffusion data, where the minor diffusion tensor eigenvalues are constrained to be equal, yielding a five-parameter model of a diffusion-weighted measurement

$$S = S_0 \exp(-\alpha b) \exp(-\beta b[\vec{g}\cdot\vec{x}]^2)\,, \tag{2}$$

where S_0 is the estimated signal at $b = 0$, $\vec{g}$ is the diffusion-weighting gradient direction, and α and β are positive scalars. The parameter of interest to us is the fiber orientation $\vec{x}$. The "nuisance parameters" are $\theta = [S_0, \alpha, \beta]$. These parameters

have Dirac priors centered on the maximum-likelihood estimate, as suggested in [8], which simplifies the calculation of the posterior distribution on the fiber orientation $\vec{x}$, given θ and the diffusion-weighted data Δ:

$$P(\vec{x},\theta|\Delta) = \frac{P(\Delta|\vec{x},\theta)P(\theta)P(\vec{x})}{P(\Delta)}\,. \tag{3}$$

The denominator in equation 3 is

$$P(\Delta) = \int_{\vec{x},\theta} P(\Delta|\vec{x},\theta)P(\theta)P(\vec{x})\,. \tag{4}$$

Because of the assumption of dirac priors on θ, the integration in equation 4 is reduced to integrating over potential orientations of $\vec{x}$. The likelihood of each diffusion-weighted measurement in Δ, given a particular $\vec{x}$ is modeled as a normal distribution with mean S (from equation 2) and variance σ^2 estimated independently from the data in each voxel [9], exactly as in [8]. The likelihood, $P(\Delta|\vec{x},\theta)$, is estimated for each of 1922 directions, evenly spread over the sphere [10]. The integral in equation 4 is approximated as the sum of the integrand, $P(\Delta|\vec{x},\theta)P(\theta)P(\vec{x})$, which is evaluated at all 1922 directions.

The key difference between [8] and the present work is that Friman et al use a fixed prior on the fiber orientation, $P(\vec{x})$, which depends on the previous direction, while in the present work we use a prior derived from the atlas. In [8], for step i in the tracking process, the prior for an orientation $\vec{x}_i$ is

$$P(\vec{x}_i) = [\vec{x}_i \cdot \vec{x}_{i-1}]^\gamma \tag{5}$$

when $[\vec{x}_i \cdot \vec{x}_{i-1}]$ is positive and zero otherwise. The parameter γ is a user-tunable parameter that is set to 1 in [8]. Thus the prior penalizes high curvature of the fiber trajectory. This prior is applied equally to all paths in the brain, which can terminate tracking prematurely in tracts with high curvature. In contrast, the atlas prior is derived from the dyadic tensor of the atlas, which reflects the degree of alignment of the local anatomy over the population. Specifically, for a voxel in the subject space where tracking takes place,

$$P(\vec{x}) = M(1/2, 3/2, \kappa)^{-1} \exp(\kappa[\vec{m} \cdot \vec{x}]^2)\,, \tag{6}$$

where $\vec{m}$ is the principal eigenvector of the dyadic tensor, i.e. the mean of the 11 fiber orientation estimates derived from the atlas, M is a normalization constant that ensures $P(\vec{x})$ integrates to unity, and κ is a scalar parameter that describes the concentration of the distribution, which is high when there is good alignment of the orientations in the atlas. We calculate $\vec{m}$ and κ from the dyadic tensors in the atlas, after warping the dyads into the subject space using the algorithm in [6]. Figure 1 shows a slice of the atlas after transformation into the subject space. The image on the left is the fractional anisotropy of the atlas mean diffusion tensor, and the image on the right shows t_1 of the dyadic tensors in the same slice.

The procedure for fitting κ given a dyadic tensor comes from Mardia and Jupp [11]. When $\kappa = 0$, the distribution is uniform. As κ increases, the prior probability density function (PDF) $P(\vec{x})$ becomes more concentrated about $\vec{m}$, with small-circle contours centered on $\pm\vec{m}$, so orientations that depart from the atlas mean are penalized more heavily when there is strong alignment of the local fiber orientation estimates from all subjects. If the dyadic tensor is oblate, as we may expect in fiber crossing regions, then κ may be negative, in which case $\vec{m}$ in equation 6 is the third eigenvector of D_y and the prior probability is maximum along the great circle normal to $\vec{m}$. In the major white matter tracts, t_1 is high and hence κ is large and positive.

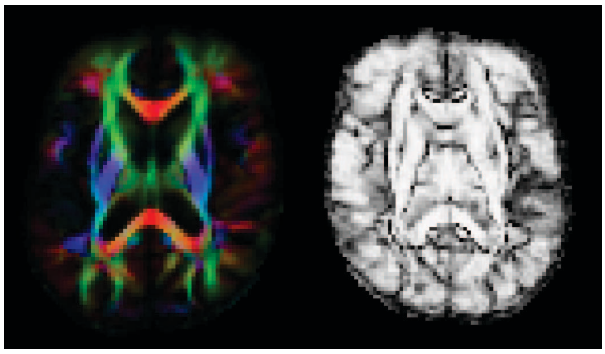

Fig. 1. Left: slice of the diffusion-tensor atlas fractional anisotropy warped into the subject space for tracking. Right: eigenvalue t_1 of the dyadic tensors from the atlas, transformed into subject space.

2.4. Probabilistic tractography

Given the posterior PDF on $\vec{x}$ in each voxel, tracking proceeds from a seed point in steps of 0.5 mm, using the interpolation scheme described in [12]. We track 1000 probabilistic streamlines from each seed point. At each step in the tracking, the local orientation of the streamline is randomly sampled from the set of 1922 directions, where the probability of selecting a vector $\vec{x}$ is determined by the posterior in equation 3. The tracking stops if the streamline reaches the surface of the brain, if it intersects itself, or if it curves by more than 80 degrees over the largest voxel dimension (2.2 mm). The tractography method, including the Bayesian PDF estimation is implemented in the open-source Camino toolkit [13].

3. RESULTS

We demonstrate the method in one subject not used in the atlas construction. Seed regions of interest (ROI) were defined manually in the image space of the subject. The connectivity of each seed ROI to another voxel in the brain is defined as the number of probabilistic streamlines that intersect the

voxel. The results are thresholded for display; connectivity greater than 1% of the total number of probabilistic streamlines in the ROI is shown. The results are rendered within the T1-weighted image of the subject using MRIcro [14]. Figure 2 shows a seed ROI placed in the fornix. This path is difficult to track because of its high curvature and proximity to other whiter matter tracts. Using a curvature prior results in a small increase in connectivity along the fiber path, but the atlas prior allows more fibers to track further along the tract. Figure 3 shows results of tracking from an ROI in the cingulum, another tract that is difficult to recover using tractography. Again, the atlas prior allows us to track further along the pathway, though there are some false-positive interhemispheric connection probabilities in all three images.

4. CONCLUSIONS

The atlas provides an anatomically-based prior that appears to improve tractography along known pathways. The prior is derived directly from the study population after normalization. The confidence assigned to the prior in each voxel is calculated from the local variability in the study population, with the prior having stronger influence when the axis of principal diffusion is well aligned across subjects. In this work, we have demonstrated tractography in a subject image that is not used in the atlas construction. The experimental results are similar when the subject is also included in the atlas construction (results not shown).

The atlas prior is specific to the local white-matter structure in the population, whereas curvature priors are typically specified once for the entire tract, regardless of local anatomy. Limitations in the present work include the small sample size, which we shall increase in future work. Another innovation, which may be possible with a larger data set, would be to use a more complex prior distribution, such as the Bingham distribution, that can model a prior PDF with elliptical contours. Future work will include permutation testing to assess the reproducibility of the atlas prior.

5. REFERENCES

[1] S Mori, Barbara J Crain, V P Chacko, , and P C M van Zijl, "Three-dimensional tracking of axonal projections in the brain by magnetic resonance imaging," *Annals of Neurology*, vol. 45, pp. 265–269, 1999.

[2] P J Basser, J Mattiello, and D Le Bihan, "Estimation of the effective self-diffusion tensor from the NMR spin echo," *Journal of Magnetic Resonance Series B*, vol. 103, pp. 247–254, 1994.

[3] P J Basser, S Pajevic, C Pierpaoli, J T Duda, and A Aldroubi, "In vivo fiber tractography using DT-MRI data," *Magnetic Resonance in Medicine*, vol. 44, pp. 625–632, 2000.

[4] O Coulon, D C Alexander, and S R Arridge, "Diffusion tensor magnetic resonance image regularization," *Medical Image Analysis*, vol. 8, pp. 47–67, 2004.

[5] H Zhang, P A Yushkevich, D Rueckert, , and J C Gee, "Unbiased white matter atlas construction using diffusion tensor images," in *International Conference on Medical Image Computing and Computer Assisted Intervention*, October 2007, pp. 211–218.

[6] H Zhang, P A Yushkevich, D C Alexander, and J C Gee, "Deformable registration of diffusion tensor MR images with explicit orientation optimization," *Medical Image Analysis*, vol. 10, pp. 764–785, 2006.

[7] P J Basser and S Pajevic, "Statistical artifacts in diffusion tensor MRI (DT-MRI) caused by background noise," *Magnetic Resonance in Medicine*, vol. 44, pp. 41–50, 2000.

[8] O Friman, G Farnebäck, and C F Westin, "A bayesian approach for stochastic white matter tractography," *IEEE Transactions on Medical Imaging*, vol. 25, pp. 965–978, 2006.

[9] R Salvador, A Peña, D K Menon, T A Carpenter, J D Pickard, and E T Bullmore, "Formal characterization and extension of the linearized diffusion tensor model," *Human Brain Mapping*, vol. 24, pp. 144–155, 2004.

[10] R H Hardin, J A Sloane, and W D Smith, "Tables of spherical codes with icosahedral symmetry," `http://www.research.att.com/~njas/icosahedral.codes/`.

[11] K V Mardia and P E Jupp, *Directional Statistics*, Wiley, 2000.

[12] T E J Behrens, M W Woolrich, M Jenkinson, H Johansen-Berg, R G Nunes, S Clare, P M Matthews, J M Brady, and S M Smith, "Characterization and propagation of uncertainty in diffusion-weighted MR imaging," *Magnetic Resonance in Medicine*, vol. 50, pp. 1077–1088, 2003.

[13] P A Cook, Y Bai, M G Hall, S Nedjati-Gilani, K K Seunarine, G J M Parker, and D C Alexander, "Camino: Open-source diffusion-MRI reconstruction and processing," in *Proceedings of the Scientific Meeting of the International Society for Magnetic Resonance in Medicine*, 2006, p. 2759.

[14] C Rorden and M Brett, "Stereotaxic display of brain lesions," *Behavioural Neurology*, vol. 12, pp. 191–200, 2000.

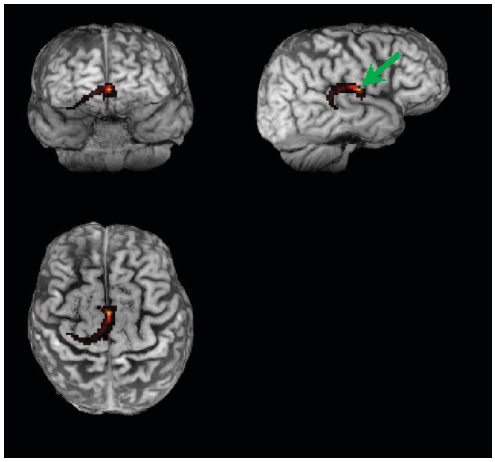

(a) Tracking with a uniform prior

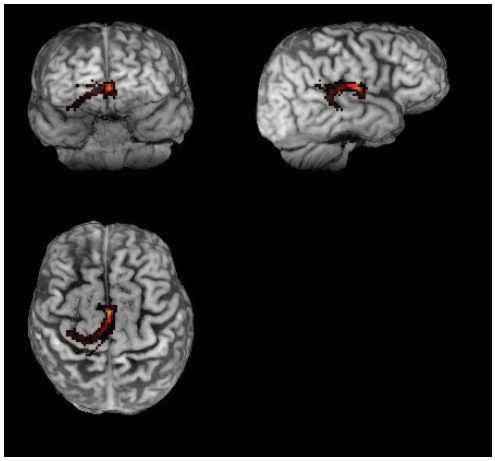

(b) Tracking with a curvature prior

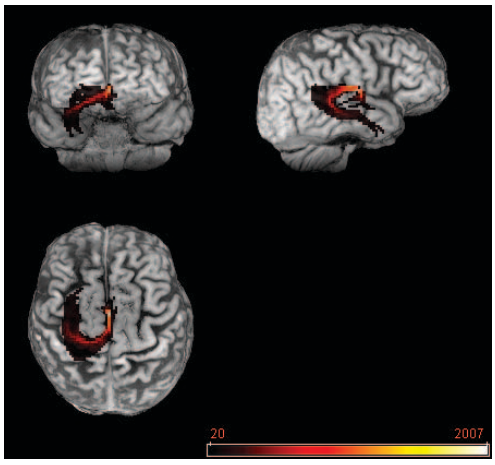

(c) Tracking with the atlas prior

Fig. 2. Results from probabilistic tracking in the left fornix. The arrow in the first figure indicates the seed point common to all images.

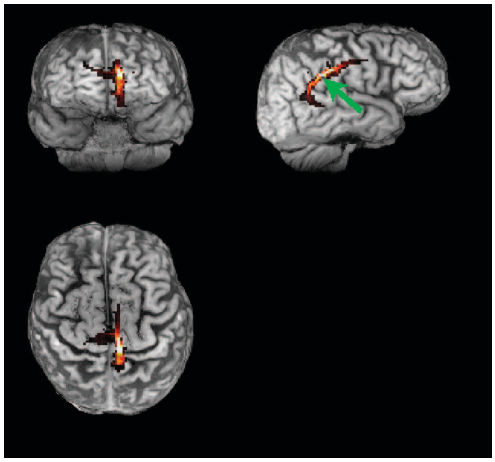

(a) Tracking with a uniform prior

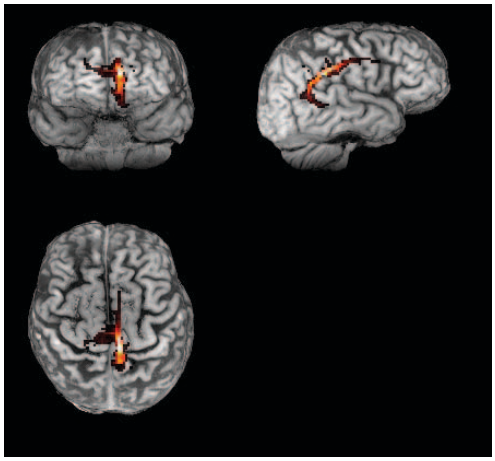

(b) Tracking with a curvature prior

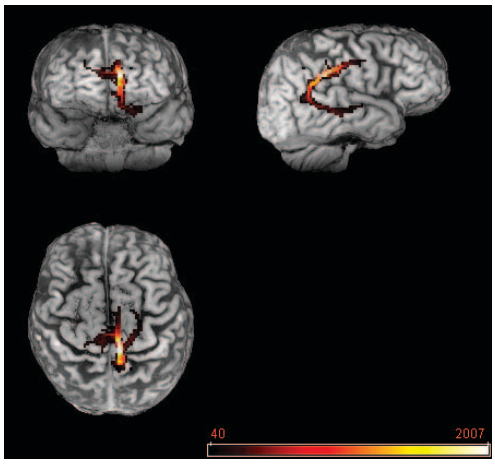

(c) Tracking with the atlas prior

Fig. 3. Results from probabilistic tracking in the right cingulum. The arrow in the first figure indicates the seed point common to all images.